Journal of Power Sources 185 (2008) 784–789

Contents lists available at ScienceDirect

Journal of Power Sources

journal homepage: www.elsevier.com/locate/jpowsour

Interaction of $La_{0.8}Sr_{0.2}MnO_3$ interlayer with $Gd_{0.1}Ce_{0.9}O_{1.95}$ electrolyte membrane and $Ba_{0.5}Sr_{0.5}Co_{0.8}Fe_{0.2}O_{3-\delta}$ cathode in low-temperature solid oxide fuel cells

Min Yang[a,b], Min Zhang[a,b], Aiyu yan[a,b], Xiangling Yue[a,b], Zhifang Hou[a], Yonglai Dong[a], Mojie Cheng[a,*]

[a] Dalian Institute of Chemical Physics, Chinese Academy of Sciences, 457 Zhongshan Road, Dalian 116023, PR China
[b] Graduate School of the Chinese Academy of Sciences, Beijing 100049, PR China

ARTICLE INFO

Article history:
Received 16 June 2008
Received in revised form 19 July 2008
Accepted 21 July 2008
Available online 30 July 2008

Keywords:
Solid oxide fuel cells
Interfacial modification
Inter-diffusion
Impedance spectroscopy
Open-circuit voltage

ABSTRACT

Low-temperature solid oxide fuel cells with a $La_{0.8}Sr_{0.2}MnO_3$ (LSM) interlayer between the $Ce_{0.9}Gd_{0.1}O_{1.95}$ (GDC) electrolyte membrane (20 μm) and the $Ba_{0.5}Sr_{0.5}Co_{0.8}Fe_{0.2}O_3$ (BSCF)–GDC composite cathode are fabricated by sintering the BSCF–GDC composite cathodes at 900, 950 and 1000 °C. The results of scanning electron microscopy/energy dispersive X-ray analysis (SEM/EDX) for a model LSM/BSCF bi-layer pellet suggest that Ba, Co and Fe in BSCF as well as La and Mn in LSM have diffused into their counter sides. The X-ray diffraction (XRD) results on the simulated cells also indicate the incorporation of La into the GDC electrolyte membrane and the mutual diffusion of elements between the LSM layer and the BSCF layer. Analysis of the impedance spectra and interfacial reaction activation energies shows that LSM interlayer accelerates the oxygen reduction. Considering a good cell performance and the highest open-circuit voltages (OCVs) at 600–500 °C, the optimum sintering temperature of BSCF–GDC composite cathode onto LSM interlayer is 900 °C.

1. Introduction

The high temperature fabrication and operation of solid oxide fuel cells (SOFCs) lead to elemental diffusions and reactions between different phases and layers, which have a great impact on the cell performances. Our previous researches on the anode-supported $La_{0.9}Sr_{0.1}Ga_{0.8}Mg_{0.2}O_{2.85}$ (LSGM)–$La_{0.45}Ce_{0.55}O_2$ (LDC) bi-layered electrolyte cell depicted that this cell had lower open-circuit voltage (OCV) and lower specific ohmic resistance than expected, which can be assigned to the diffusion of Co from $La_{0.6}Sr_{0.4}CoO_3$ (LSC) cathode to LSGM electrolyte [1–3]. A work on an all-perovskite fuel cell done by Tao et al. [4] suggested that a slight cross-diffusion at the interfaces between different perovskite components might improve the interfacial contact and decrease the interfacial resistance. La cations could diffuse into yttria-stabilized zirconia (YSZ) electrolyte from Sr-doped lanthanum manganite (LSM) cathode, which lowered the cathode performance [5,6]. $Ba_{0.5}Sr_{0.5}Co_{0.8}Fe_{0.2}O_{3-\delta}$ (BSCF)–$LaCoO_3$ (LC) composite cathode had the higher electronic conductivity than the single BSCF cathode because of the solid-state reaction between BSCF and LC [7].

Recently, we fabricated a low-temperature solid oxide fuel cell with a $La_{0.8}Sr_{0.2}MnO_3$ (LSM) interlayer between $Ce_{0.9}Gd_{0.1}O_{1.95}$ (GDC) electrolyte membrane and $Ba_{0.5}Sr_{0.5}Co_{0.8}Fe_{0.2}O_{3-\delta}$ (BSCF)–GDC composite cathode, and this cell showed the improved cell performance than the unmodified one [8]. In this cell, the elemental diffusion from BSCF cathode to LSM interlayer seems to play an important role. Of course, at a specific sintering temperature of LSM interlayer, the interaction between LSM and BSCF depends on the sintering temperature of the BSCF–GDC composite cathode. In this paper, the interaction between LSM interlayer and GDC electrolyte as well as BSCF cathode is investigated, and its effects on cell performance are elucidated.

2. Experimental

2.1. Materials synthesis and cell fabrication

The home-made BSCF, LSM and GDC powders were synthesized by the sol–gel process. Anode-supported thin electrolyte (20 μm) bi-layer assemblies were fabricated using a dual dry-pressing method. The anode, consisted of a 50:50 wt.% mixture of NiO and

* Corresponding author. Tel.: +86 411 84379049; fax: +86 411 84379049.
E-mail address: mjcheng@dicp.ac.cn (M. Cheng).

0378-7753/$ – see front matter © 2008 Elsevier B.V. All rights reserved.
doi:10.1016/j.jpowsour.2008.07.054

GDC powders was dry-pressed into a pellet, and then an appropriate amount of the GDC electrolyte powder was distributed on the anode surface and co-pressed with the anode using a uniaxial die-press (Ø25 mm). The resultant bi-layer was sintered at 1420 °C for 4 h. The LSM slurry was coated onto GDC electrolyte membrane surface, and fired at 1300 °C for 2 h to form a LSM interlayer. A 30 wt.% GDC-containing BSCF cathode slurry was coated on the LSM film and fired at 900, 950 and 1000 °C for 2 h, and these cells were identified as LSM-900, LSM-950 and LSM-1000, respectively. For comparison, the same cathode slurry was also coated directly onto the GDC electrolyte membrane and fired at 950 °C for 2 h, and this cell was 0-950. The geometrical area of all the cathodes was 0.5 cm^2.

2.2. Characterization of elemental diffusion

Two techniques were used for the investigation of elemental inter-diffusion and phase reactions: scanning electron microscopy/energy dispersive X-ray (SEM/EDX) analysis of a model LSM/BSCF bi-layer pellet and the reaction products detected by X-ray diffraction (XRD) on the simulated cells of the NiO–GDC/GDC assembly coated with thin layers of LSM and BSCF. The model bi-layer LSM/BSCF pellet was prepared through pressing the LSM pellet at 202 MPa and sintering at 1300 °C for 2 h. Then the BSCF slurry was deposited onto the LSM surface, followed by firing at 900 °C for 2 h. Quantitative EDX line scan measurement across the interface was carried out through a SEM equipped with EDX detector (FEI, QUANTA 200 FEG). The samples for the XRD investigations were fabricated as follows: the GDC electrolyte membrane surface of the sintered NiO–GDC/GDC assembly was coated with the LSM slurry and fired at 1300 °C for 2 h, and then the BSCF slurry was coated on the LSM film and fired at 900, 950 and 1000 °C for 2 h. The BSCF slurry was also applied to the GDC electrolyte membrane surface and fired at 950 °C for 2 h as a reference sample. The XRD measurements were performed in the 2θ range of 20–50° on a Rigaku D/max-2500PC X-ray diffractometer at 40 kV and 300 mA using Cu Kα radiation.

2.3. Electrochemical measurement

I–V measurements of single cells were carried out at 600–500 °C after the in situ reduction of the NiO anode in H_2 at 700 °C for several hours. The detailed single cell configuration has been described elsewhere [9]. Humidified H_2 (100 ml min^{-1}) and air (200 ml min^{-1}) were supplied as fuel and oxidant, respectively. The impedances were measured typically under open-circuit conditions using a Solartron 1287 potentiostat and 1260 frequency response analyzer. The frequency range was from 0.1 Hz to 10 kHz with signal amplitude of 10 mV. After testing, the cell was cooled down to room temperature under a flow of humidified hydrogen to the anode and oxygen to the cathode.

3. Results and discussion

3.1. Elemental inter-diffusion of LSM interlayer with GDC electrolyte and BSCF cathode

3.1.1. SEM/EDX analysis of a model LSM/BSCF bi-layer pellet

Information on the possible elemental inter-diffusion between LSM interlayer and BSCF cathode layer can be provided by examining a model LSM/BSCF bi-layer pellet through microanalysis. Fig. 1a shows the microstructure of the model LSM/BSCF pellet. It can be observed that the pellet is not densely sintered after the thermal treatment. For this reason, the elemental profiles presented in Fig. 1b can only be used for semi-quantitative statements. As shown in Fig. 1b, a distinct congregation of all the metal elements can be identified at the interface of LSM/BSCF bi-layer pellet. The intensities of Ba, Co, Fe decay gradually from the interface to LSM layer, and La and Mn behave similarly. The EDX line scan results confirm the elemental inter-diffusion between LSM layer and BSCF layer.

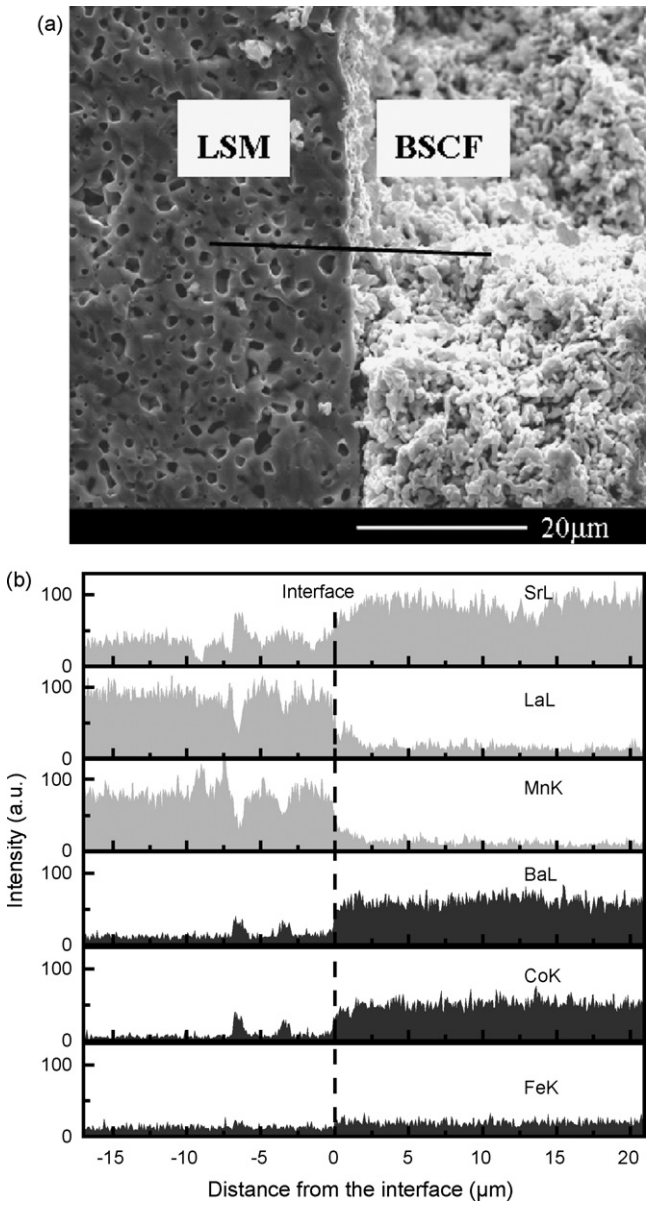

Fig. 1. (a) Microstructure and (b) line scan analysis of the materials pair LSM/BSCF.

3.1.2. X-ray diffraction on the simulated cells

The resultant X-ray diffraction patterns on the simulated cells with thin layers of LSM and BSCF are shown in Fig. 2a. To show the changes occurring in the XRD patterns more clearly, the magnified patterns between 27 and 34° are given in Fig. 2b. Line III stands for XRD results of LSM layer sintered onto GDC electrolyte membrane at 1300 °C. Lines V, VI and VII depict those of BSCF layer sintered onto LSM layer at 900, 950 and 1000 °C, respectively. XRD spectra of GDC electrolyte membrane (line I), LSM powder (line II) and BSCF cathode fired onto the GDC electrolyte at 950 °C (line IV) are also given as references.

As can be seen from line III, the main peaks, both from LSM and GDC, do show the shift to lower 2θ angles than their pure

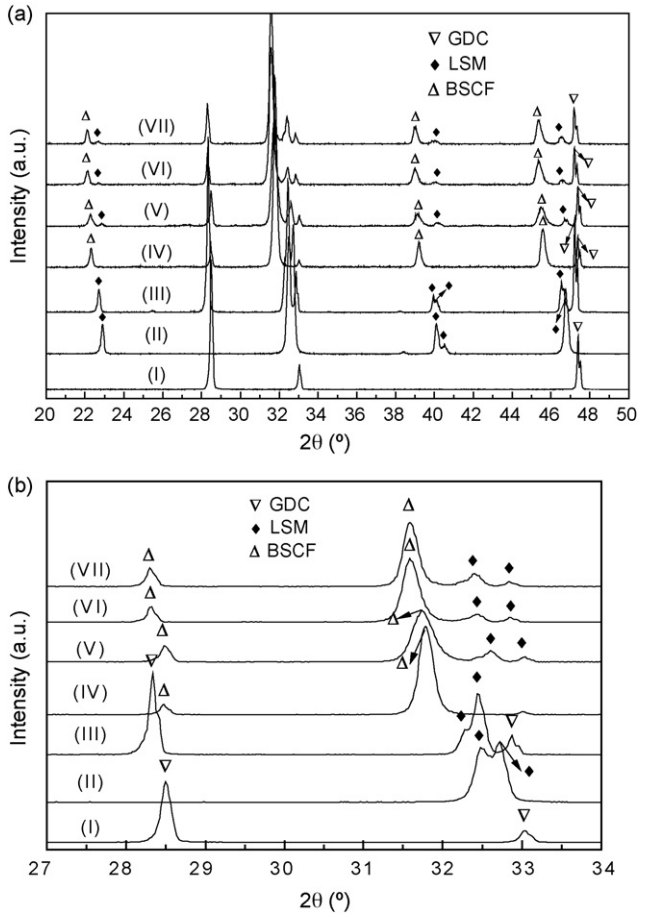

Fig. 2. (a) Complete and (b) selected XRD patterns of GDC electrolyte (I), LSM powder (II), LSM fired on GDC electrolyte at 1300 °C (III), BSCF fired on GDC electrolyte at 950 °C (IV), BSCF fired on LSM film at 900 °C (V), 950 °C (VI), and 1000 °C (VII).

phases, indicating that the solid-state reaction between them has happened when LSM layer was fired onto GDC electrolyte membrane at 1300 °C. The shift of GDC electrolyte peaks is caused by the incorporation of La^{3+} into ceria crystal lattice (La^{3+} has a larger ionic radius than Gd^{3+}), as convinced by many authors [10–13]. La-site deficiency in LSM perovskite lattice brings in the weakening of the attraction forces between ions, which results in an increase of the interatomic distance and the subsequent peak shift. Kostogloudis et al. [14] also found the increase of lattice constant for A-site deficient $Pr_{0.75}Sr_{0.2}Co_{0.2}Mn_{0.8}O_{3-\delta}$.

Increasing the sintering temperature of BSCF onto LSM layer from 900 to 950 °C, the main peaks of BSCF shift continuously to lower 2θ angles (lines V and VI) as compared with BSCF pure phase (line IV), indicating the lattice expansion in BSCF. Nevertheless, further increasing of the sintering temperature of BSCF to 1000 °C displays no further peak shift (line VII). Tai et al. [15] attributed the lattice expansion associated with the formation of oxygen vacancies upon heating $La_{0.8}Sr_{0.2}Co_{1-y}Fe_yO_3$ to: (1) the repulsion force arising between those mutually exposed cations when oxygen ions are extracted from the lattice; (2) the increase in cation size due to the reduction of the Fe and Co ions from higher to lower valences, which must occur concurrently with the creation of oxygen vacancies in order to maintain electrical neutrality. When BSCF was sintered onto LSM layer at 900 °C, the emigrated cations of Ba, Co and Fe from BSCF exceeded the incorporated cations of La and Mn into BSCF (as indicated from Fig. 1), causing a charge imbalance. In order to maintain electrical neutrality of BSCF, the creation of oxygen vacancies and a simultaneous reduction of Co and Fe species will occur, causing the shift of BSCF main peaks. The diffusions of La and Mn from LSM to BSCF can compensate the cations depletion in BSCF to some extent. According to the peaks change of BSCF cathode, it is concluded that this compensate effect is less evident at the BSCF sintering temperature of 900 and 950 °C. When BSCF is sintered at 1000 °C, more La and Mn will diffuse into BSCF from the LSM layer and the compensate effect is strengthened, leaving its peaks shift less obviously. The peak shift of LSM when BSCF was sintered onto its surface is also caused by their inter-diffusion.

3.2. Electrochemical impedance spectra (EIS) analysis

Impedance spectra of 0-950, LSM-900, LSM-950 and LSM-1000 at 600–500 °C are shown in Fig. 3a–c. At 600 °C, the impedance spectrum of 0-950 shows one dominating arc (~100 Hz) at medium frequency (MF). In accordance with literatures [16,17], this MF feature can be assigned to the electrochemical oxygen surface exchange reaction (in cathodic direction): oxygen adsorption at the electrode surface, oxygen dissociation, ionization, and incorporation into vacancies of the mixed conducting electrode. When LSM interlayer is introduced, the corresponding arcs decrease in the spectra, no matter what the sintering temperature of the cathode is. Furthermore, this arc is largest and the smallest for LSM-950 and LSM-1000 respectively among the spectra of LSM modified cells. The additional oxygen vacancies in BSCF generated from the charge imbalance improve the adsorption and dissociation of oxygen molecules on cathode surface, and therefore are beneficial for oxygen surface exchange reaction. However, the increase in oxygen vacancies will bring forth a concomitant decrease in electronic conductivity [15,18], which is harmful to oxygen ionization and hence more prone to slow down this process. When the cathode is sintered at 900 °C, an increase in the number of oxygen vacancies in BSCF bulk may be overwhelming, leading to the subdued arc size. Whereas when the cathode is treated at 950 °C, the stagnant ionization step seems to be significant. The features of BSCF can also be modified by the diffusion of La and Mn. La doped BSCF is advantageous to the oxygen adsorption/desorption and the oxygen ions diffusion in the cathode [19]. As indicated in the XRD results, the modified effect is evident when the cathode was sintered at 1000 °C. Since the arc at 100 Hz is notably reduced from the impedance spectrum of LSM-1000, it can be deduced that the diffusion of La and Mn is beneficial to the oxygen surface exchange.

Another noticeable aspect when LSM interlayer was introduced is that an additional MF arc at relatively high frequency (with the summit frequencies of 200 Hz) can be observed in the spectra of LSM-900. The appearance of this arc is not clear, but taking that the consumption of Co and Fe from cathode may hold back the oxygen ionic mobility [20] and thus incline to lower the oxide ion conductivity, we tentatively presume that it is coupled with the transportation of oxygen ions through the cathode. Evidently, higher sintering temperature of cathode drives more consumption of Co and Fe in BSCF cathode. Thus this arc increases in magnitude when the cathode is subjected from 900 to 950 °C. The evident decrease of this arc in the spectrum of LSM-1000 can be attributed to the diffusion of La and Mn.

The low frequency (LF) arc centered at approximate 5 Hz has appeared from the impedance spectrum of LSM-900 as compared with that of 0-950. With the increasing sintering temperature of the cathode, the corresponding arc decreases in the impedance of LSM-950, and then disappears from the impedance of LSM-1000. Many researchers have found that the diffusion of Co and Fe cations into LSM is in favor of the increasing of oxygen vacancy concentration and electrical conductivity as well as oxygen mobility [21–23]. Furthermore, the presence of alkaline earth elements at the surface

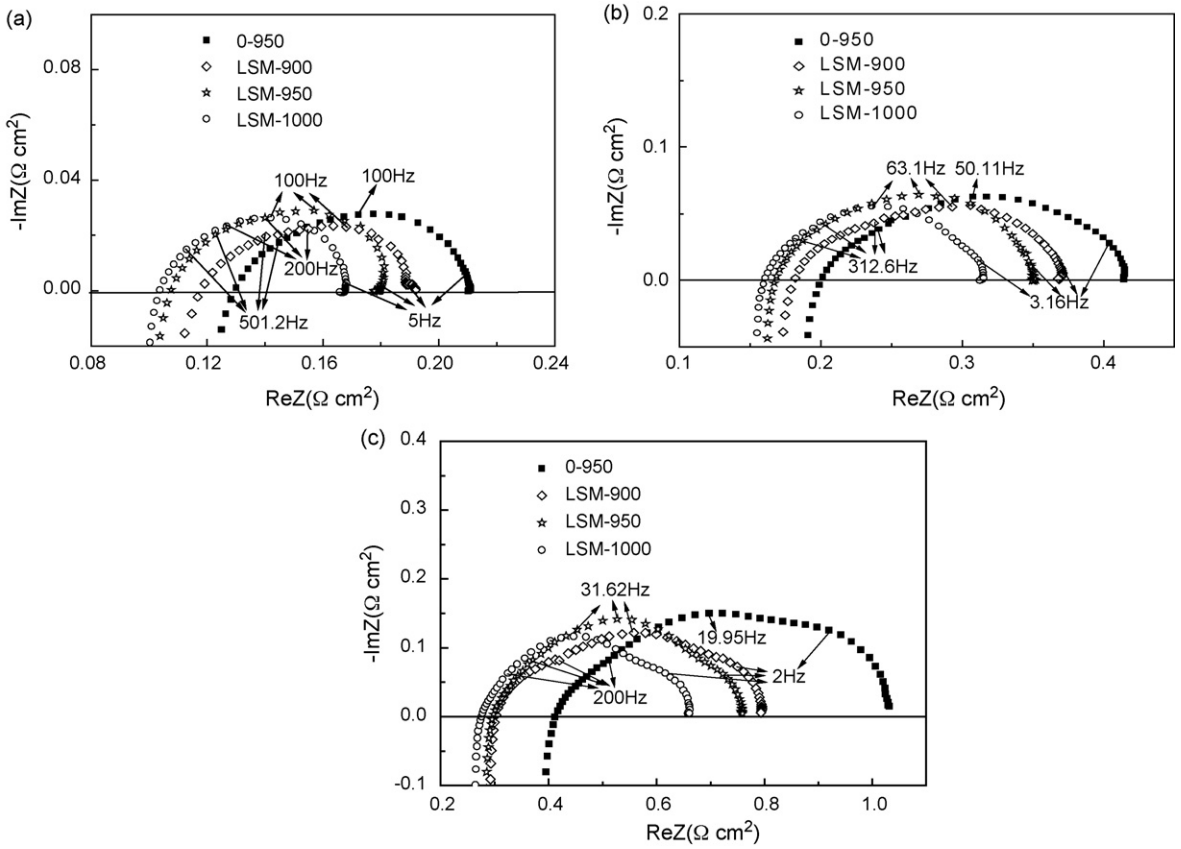

Fig. 3. Electrochemical impedance spectra of 0-950, LSM-900, LSM-950 and LSM-1000 measured at 600 °C (a), 550 °C (b), and 500 °C (c) under open circuit.

seems to have a beneficial effect on the oxygen exchange kinetics [24–26]. Therefore, the LSM interlayer would benefit from the incorporation of Ba, Co and Fe in terms of oxygen reduction reaction. Thus, the yielded and gradually decreased LF impedance when adding the LSM interlayer can be attributed to the oxygen reduction at the "new LSM interlayer". A high frequency (HF) arc at 501.2 Hz can also be detected in the impedance of 0-950, although this HF arc is not evident. Due to the good interfacial contact and the increased cathode reaction sites at the cathode/electrolyte interface when LSM interlayer was added, the HF arc decreases with increasing sintering temperature of BSCF–GDC composite cathode.

As the measurement temperature falls off, the HF and LF arcs are more prominent, and only one MF arc (the characteristic frequencies are around 63.1 and 31.62 Hz respectively at 550 and 500 °C) can be identified from the impedance spectra. However, the variation trends of impedance spectra are analogous to those of 600 °C.

The development of activation energies when LSM interlayer is present can be acquired from Fig. 4, which shows the Arrhenius plots of total interfacial polarization resistance R_p (calculated according to Ref. [27]) for single cells with and without the LSM interlayer. Good linearity of $\ln(R_p{}^{-1})$ versus reciprocal temperature is observed in the investigated temperature range. The activation energy for 0-950 derived from Fig. 4 is 106.1 kJ mol^{-1}, suggesting that oxygen surface exchange process of BSCF is the rate limiting step [28]. When LSM interlayer is added, the activation energies descend with increasing cathode treatment temperatures, and the corresponding values are reduced to 97.8, 95.7 and 91.5 kJ mol^{-1} for LSM-900, LSM-950, and LSM-1000, respectively. As the anode–electrolyte assembly is prepared through the same procedures, their interfaces are assumed to be the same. Thereby, it can be concluded that adding LSM interlayer speeds up oxygen reduction reactions, and the trend is driven up by increasing sintering temperature of the cathode. The phase interactions when the LSM interlayer exists may hopefully contribute to the decreased activation energies.

3.3. Cell performance, open-circuit voltage and long-term stability

In Fig. 5a–d, the *I–V* and *I–P* curves of 0-950, LSM-900, LSM-950 and LSM-1000 are given. At sufficiently high current densities the concentration polarization can be found at 600 °C, which is

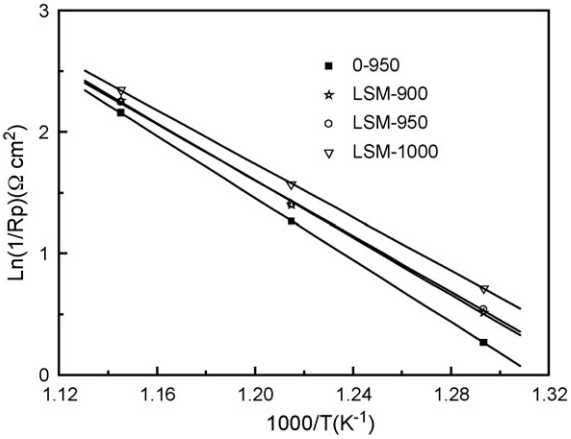

Fig. 4. Arrhenius plots of cathode/electrolyte interfacial resistances for 0-950, LSM-900, LSM-950 and LSM-1000.

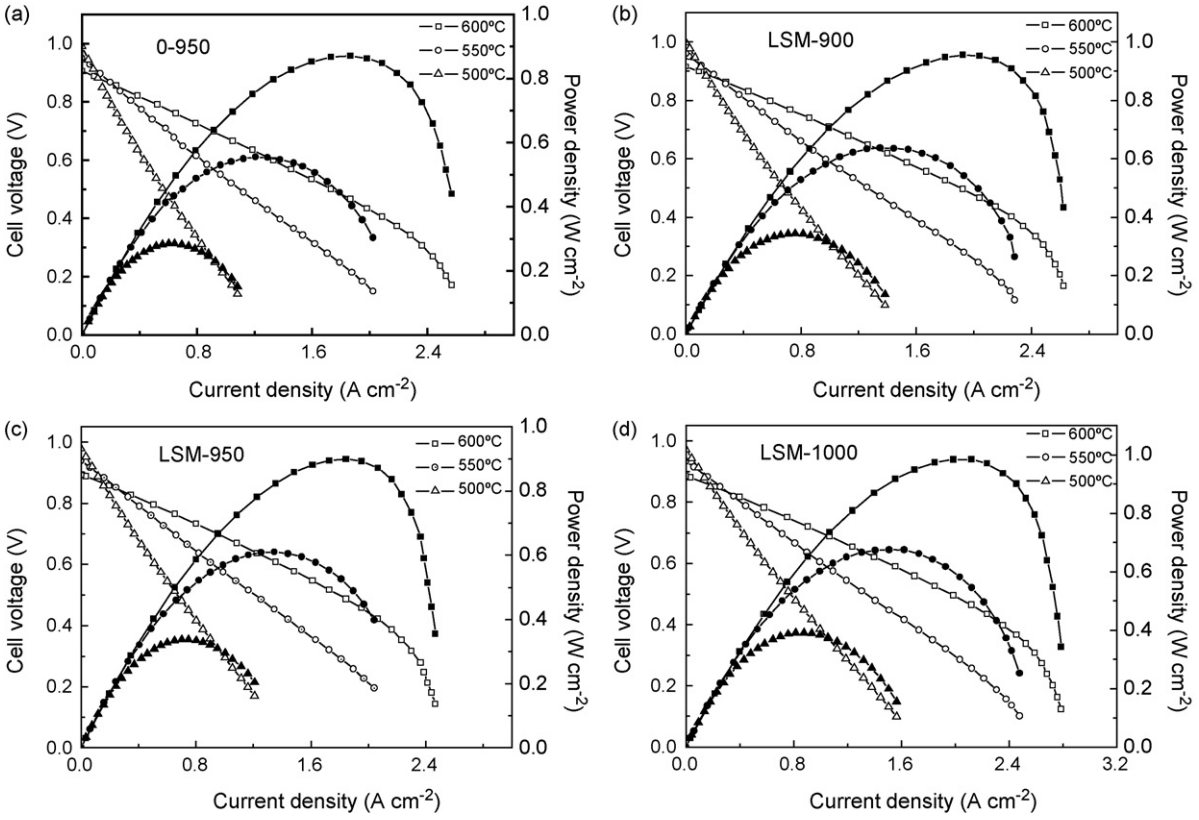

Fig. 5. *I–V* curves and power densities at 600–500 °C for 0-950 (a), LSM-900 (b), LSM-950 (c), and LSM-1000 (d).

Table 1
Comparison of OCV values

Temperature (°C)	OCV (V)			
	0-950	LSM-900	LSM-950	LSM-1000
600	0.905	0.916	0.894	0.885
550	0.95	0.96	0.938	0.933
500	0.99	0.998	0.978	0.972

attributed to the low porosity of the anode in view that the anode consists of 50 wt.% NiO and 50 wt.% GDC. Within the tested temperature range, the highest power densities of the single cells decrease in sequence of LSM-1000, LSM-900, LSM-950 and 0-950. At 600 °C, their maximum power densities are 0.985, 0.955, 0.9 and 0.87 W cm^{-2}, respectively.

The OCV values obtained in this study are summarized in Table 1. Compared with the OCVs of 0-950, the corresponding values increase for LSM-900, and then continuously decrease with the increase of the sintering temperature of the cathode. In this study, the change of interfacial electronic conductivity must be taken into consideration in discussing the OCV values. The incorporation of La into GDC electrolyte membrane reduces the interfacial electronic conductivity and thus depresses the internal short circuit current in GDC electrolyte membrane, while the incorporation of Co and Fe into the LSM interlayer has the reverse effect. From the OCV values listed in Table 1, it can be concluded that the former effect is overwhelming when the cathode is sintered at 900 °C, while the latter effect is dominant at higher sintering temperature of the cathode.

Although substantial cathode improvements are still necessary to facilitate the increase of power densities for low-temperature SOFCs, an equally important goal is the long-term stability of the cells. In vision that LSM-900 has both the highest OCVs and satisfactory cell performance, it is considered as the optimum cell in this study. Fig. 6 illustrates the long-term operation of LSM-900 at 600 °C under a constant voltage of 0.65 V using humidified hydrogen as fuel and air as oxidant, respectively. The relatively stable performance within the first 50 h is observed for this cell, and then it decreases slowly in the next 50 h. The cell attenuations are 5.2 and 7.9% respectively in the first and second 50 h. Long-term cell performance can be affected by many factors, such as the reducibility of the ceria-based ceramics in the anode substrate and electrolyte, changes of electrical conductivity and porosity due to slowly sintering of anode, reaction of alkaline earth with carbon dioxide in air, phase interaction under the condition of cell operation, and so on.

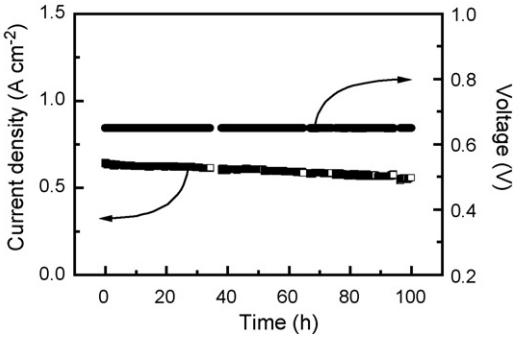

Fig. 6. Long-term data of LSM-900 at 600 °C under a constant voltage of 0.65 V.

4. Conclusions

Low-temperature SOFCs with LSM interlayer between GDC electrolyte membrane and $Ba_{0.5}Sr_{0.5}Co_{0.8}Fe_{0.2}O_3$ (BSCF)–GDC cathode were fabricated at the cathode sintering temperature of 900, 950 and 1000 °C. The EDX line scan analysis of a model LSM/BSCF double layer identified the transport of Co, Ba and Fe from BSCF into LSM, and simultaneous migration of Mn and La from LSM to BSCF. XRD results also suggested the inter-diffusion between LSM interlayer and GDC electrolyte as well as BSCF cathode. LSM interlayer accelerated the cathode reaction processes, as concluded from the impedance spectra and the continuously decreased interfacial reaction activation energies with the increase of the sintering temperature of the cathode. Benefit from the interaction effect, the performance of the LSM modified cell (when the cathode was sintered at 1000 °C) under operation of air and humidified H_2 reaches 0.39 W cm^{-2} at 500 °C, which is about 1.4-fold higher than the unmodified one. The cell with a LSM interlayer and the BSCF–GDC composite cathode sintered at 900 °C showed the promising performance (0.955 W cm^{-2}) and the highest OCVs (0.916 V) at 600 °C, and was considered as the optimum cell. The longevity data of this cell in 100 h indicated that it attenuated slowly at the first 50 h.

Acknowledgements

The authors gratefully acknowledge financial supports from the Ministry of Science and Technology of China (nos. 2004CB719506, 2005CB221404 and 2006AA05Z147), National Natural Science Foundation of China (Grant No. 20676132) and Europe Commission (SOFC 600). Also Min Yang wishes to thank Junbo Hou for useful discussion.

References

[1] Z.H. Bi, M.J. Cheng, Y.L. Dong, H.J. Wu, Y.C. She, B.L. Yi, Solid State Ionics 176 (2005) 655–661.
[2] Z.H. Bi, Y.L. Dong, M.J. Cheng, B.L. Yi, J. Power Sources 161 (2006) 34–39.
[3] Z.H. Bi, Ph.D. Thesis, Dalian Institute of Chemical Physics, Chinese Academy of Sciences, Dalian, P.R. China, 2005.
[4] S.W. Tao, J.T.S. Irvine, J.A. Kilner, Adv. Mater. 17 (2005) 1734–1737.
[5] C. Clausen, C. Bagger, J.B. Bilde-Sørensen, A. Horsewell, Solid State Ionics 70/71 (1994) 59–64.
[6] A. Mitterdorfer, L.J. Gauckler, Solid State Ionics 111 (1998) 185–218.
[7] W. Zhou, Z.P. Shao, R. Ran, P.Y. Zeng, H.X. Gu, W.Q. Jin, N.P. Xu, J. Power Sources 168 (2007) 330–337.
[8] M. Yang, M. Zhang, X.L. Yue, A.Y. Yan, Z.F. Hou, Y.L. Dong, M.J. Cheng, Electrochem. Solid-State Lett. 11 (3) (2008) B34–B37.
[9] M. Yang, A.Y. Yan, M. Zhang, Z.F. Hou, M.J. Cheng, J. Power Sources 175 (2008) 345–352.
[10] A. Naoumidis, A. Ahmad-Khanlou, Z. Samardzija, D. Kolar, Fresenius J. Anal. Chem. 365 (1999) 277–281.
[11] A.L. Shaula, V.V. Kharton, F.M.B. Marques, A.V. Kovalevsky, A.P. Viskup, E.N. Naumovich, J. Solid State Electrochem. 10 (2006) 28–40.
[12] H. Inaba, H. Tagawa, Solid State Ionics 83 (1996) 1–16.
[13] K. Eguchi, T. Setoguchi, T. Inoue, H. Arai, Solid State Ionics 52 (2000) 165–172.
[14] G.Ch. Kostogloudis, Ch. Ftikos, A. Ahmad-Khanlou, A. Naoumidis, D. Stöver, Solid State Ionics 134 (2000) 127–138.
[15] L.-W. Tai, M.M. Nasrallah, H.U. Anderson, D.M. Sparlin, S.R. Schlin, Solid State Ionics 76 (1995) 259–271.
[16] F.S. Baumann, J. Fleig, H.-U. Habermeier, J. Maier, Solid State Ionics 177 (2006) 3187–3791.
[17] M.J. Jørgensen, M. Mogensen, J. Electrochem. Soc. 148 (2001) A433–A442.
[18] L.-W. Tai, M.M. Nasrallah, H.U. Anderson, D.M. Sparlin, S.R. Schlin, Solid State Ionics 76 (1995) 273–283.
[19] S. Li, Z. Lü, X. Huang, B. Wei, W. Su, J. Phys. Chem. Solids 68 (2007) 1707.
[20] N. Trofimenko, H. Ullmann, Solid State Ionics 118 (1999) 215–227.
[21] K.T. Lee, A. Manthiram, Chem. Mater. 18 (2006) 1621–1626.
[22] S. Carter, A. Selcuk, R.J. Chater, J. Kajda, J.A. Kilner, B.C.H. Steele, Solid State Ionics 53–56 (1992) 597–605.
[23] S.P.S. Badwal, S.P. Jiang, J. Love, J. Nowotny, M. Rekas, E.R. Vance, Ceram. Int. 27 (2001) 419–429.
[24] S. McIntosh, J.F. Vente, W.G. Heije, D.H.A. Blank, H.J.M. Bouwmeester, Chem. Mater. 18 (2006) 2187–2193.
[25] C. Argirusis, S. Wagner, W. Menesklou, C. Warnke, T. Damjanovic, G. Borchardt, E. Ivers-Tiffee, Phys. Chem. Chem. Phys. 7 (2005) 3523–3525.
[26] F.S. Baumann, J. Fleig, M. Konuma, U. Starke, H.-U. Habermeier, J. Maier, J. Electrochem. Soc. 152 (2005) A2074–A2079.
[27] M.L. Liu, H.X. Hu, J. Electrochem. Soc. 143 (1996) L109–L112.
[28] Z.P. Shao, S.M. Haile, Nature 431 (2004) 170–173.